Supplementary Information

Dipole patterns in tropical precipitation were pervasive across landmasses throughout Marine Isotope Stage 5

Katrina Nilsson-Kerr[1*], Pallavi Anand[1], Philip B. Holden[1], Steven C. Clemens[2], Melanie J. Leng[3,4].

[1]School of Environment, Earth and Ecosystem Sciences, Faculty of STEM, The Open University, Walton Hall, MK7 6AA Milton Keynes, United Kingdom. [2]Department of Geological Sciences, Brown University, RI 02912 Providence, United States of America. [3]Environmental Science Centre, British Geological Survey, NG12 566 Nottingham, United Kingdom. [4]School of Biosciences, University of Nottingham, LE12 5RD Loughborough, United Kingdom.

Corresponding author: [1]Katrina Nilsson-Kerr, k.nilsson-kerr@hw.ac.uk

*Present address: The Lyell Centre, Heriot-Watt University, EH14 4BA Edinburgh, United Kingdom.

This PDF file includes:

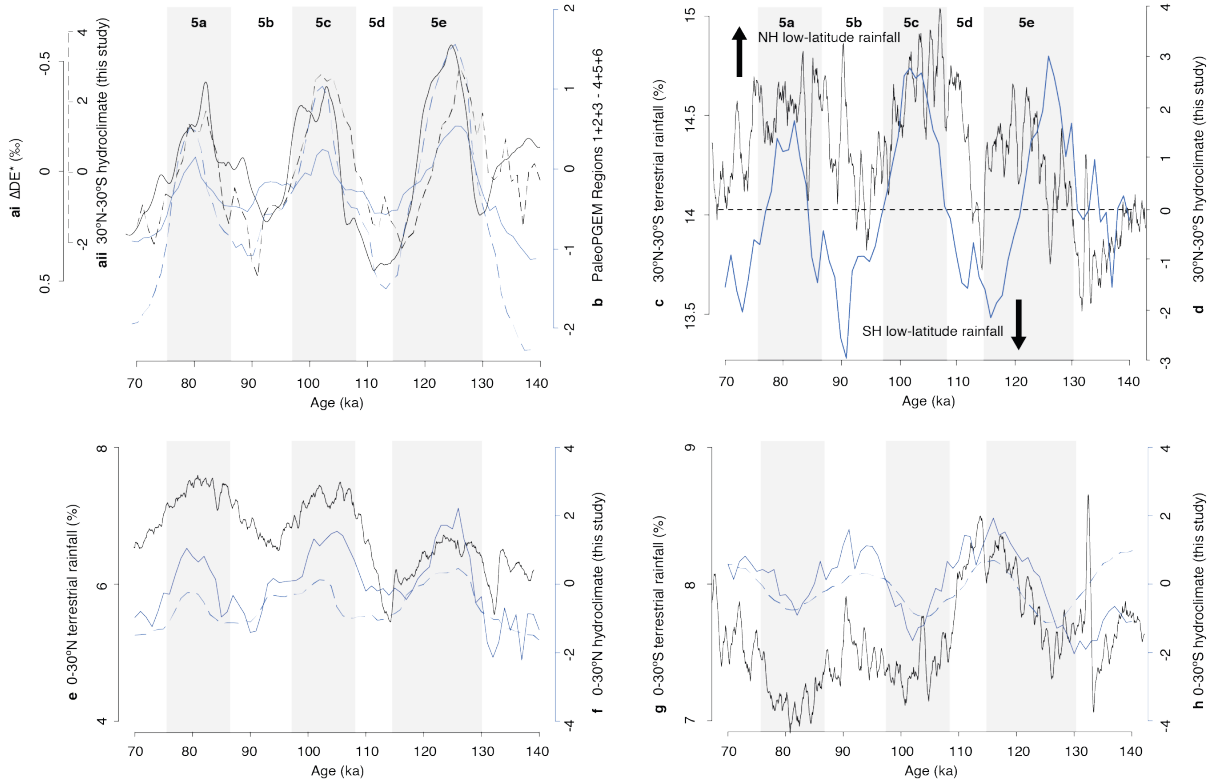

Supplementary Figure 1. Northern hemisphere and southern hemisphere hydroclimate proxy-model comparisons (**a i**) Dole effect [1] (solid black line) (**a ii**) 30ºN-30ºS compiled hydroclimate proxy data (this study; dashed black line) (**b**) PaleoPGEM 30ºN-30ºS, dashed blue line represents terrestrial only rainfall whilst solid blue line represents total rainfall (this study) (**c**) CCSM3 30ºN-30ºS terrestrial rainfall percent (solid black line) [1] (**d**) 30ºN-30ºS compiled hydroclimate proxy data (this study; blue) (**e**) CCSM3 0-30ºN terrestrial rainfall percent (solid black line) [1] (**f**) 0-30ºN compiled hydroclimate proxy data (this study; solid blue line) and PaleoPGEM 0-30ºN (this study; dashed blue line) (**g**) CCSM3 0-30ºS terrestrial rainfall percent [1] (**h**) 0-30ºN compiled hydroclimate proxy data (this study; solid blue line) and PaleoPGEM 0-30ºN (this study; dashed blue line). In order to limit bias in our regional approach we area-weight the signal from each respective region from this study to represent total northern hemisphere (0-30ºN) and southern hemisphere (0-30ºS).

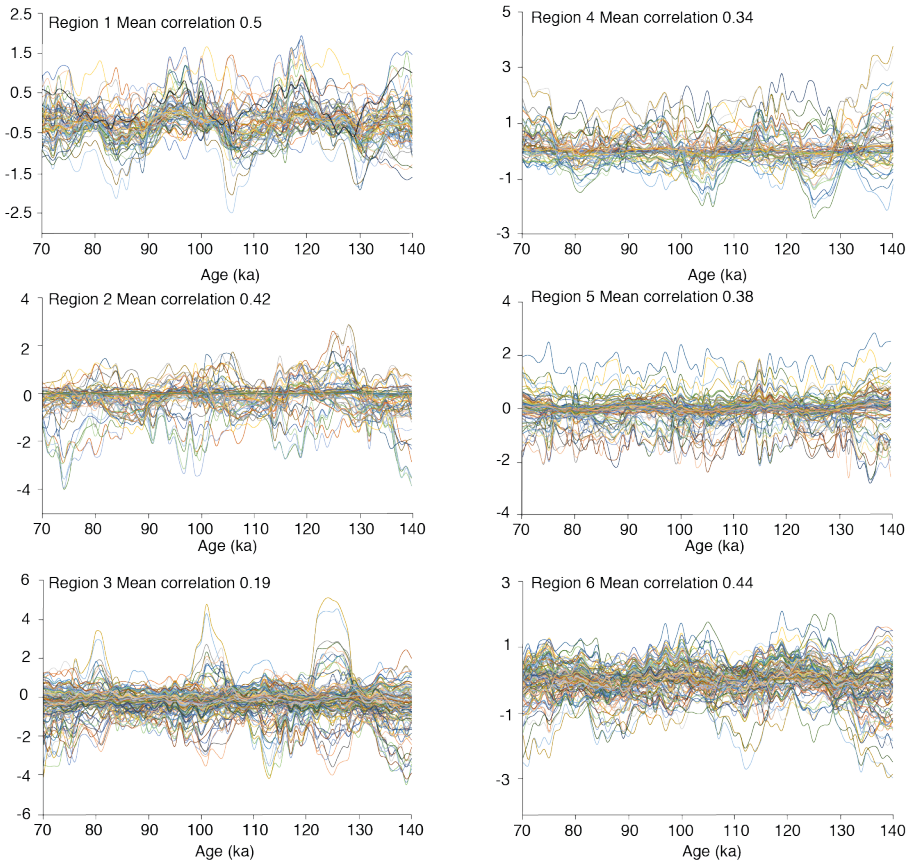

Supplementary Figure 2. Individual grid-cell emulations of precipitation change within each region. The 'mean correlation' is the average of the correlations between these individual grid-cells and the mean of all grid-cells within that region. A high correlation indicates that the local (grid-cell) responses tend to be in phase with one another. In Region 3, the responses of many grid-cells are in anti-phase, and so the mean correlation is close to zero.

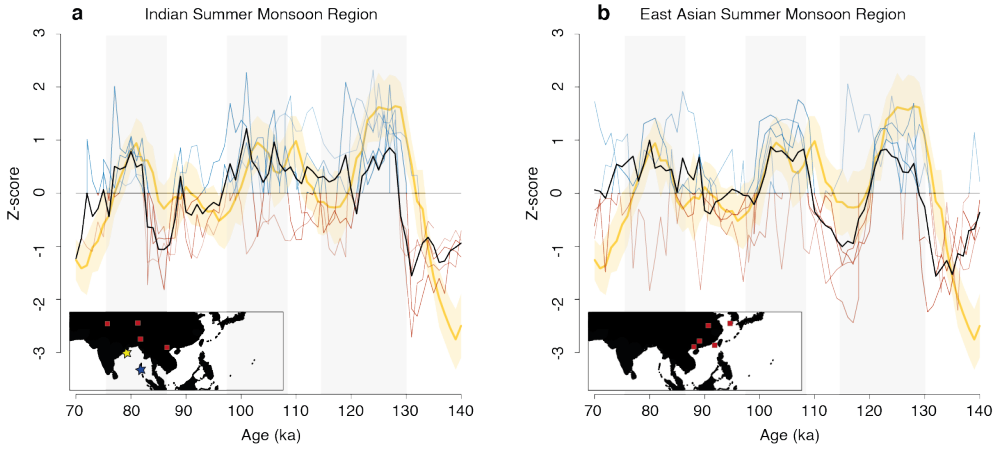

Supplementary Figure 3. Time-series proxy and emulation comparison across Region 3. Divided into the ISM (**a**) and EASM (**b**) dominated-realms, as inferred in the original studies (Supplementary Data 1). The emulated PaleoPGEM precipitation is shown in yellow with yellow shading representing the 95% confidence limit. The black line represents the average of all proxy data in each respective realm. The z-scores represent the deviation from the mean of each proxy record, with blue representing "wetter" and red "drier". Each plot contains inset map showing red squares for the location of published proxy records and the location of two new records generated in this study are shown as colored stars (See Methods, Supplementary Data 1). Grey shaded bars represent the warm sub-stages of MIS 5 (MIS 5e, c and a).

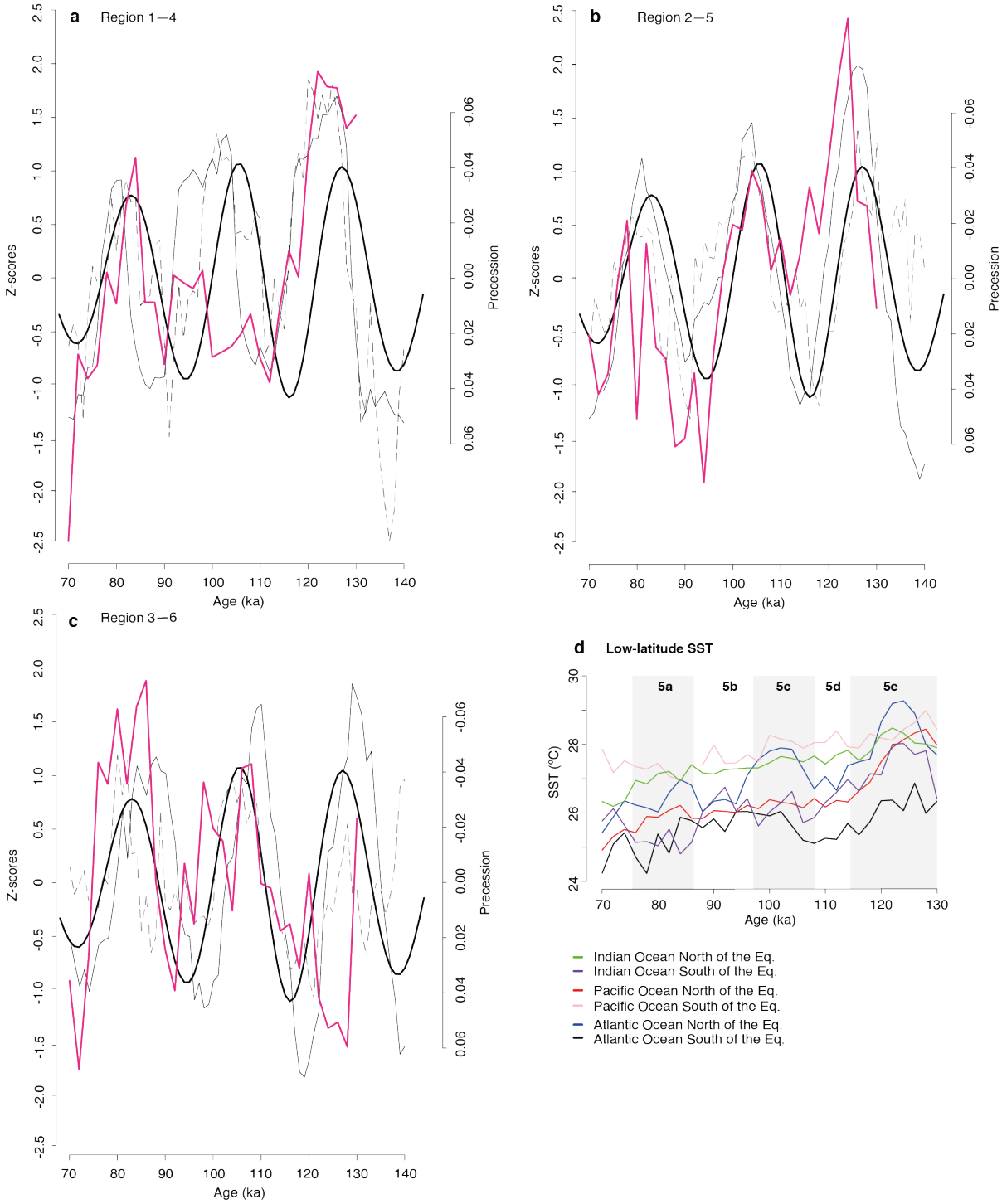

Supplementary Figure 4. Low-latitude inter-hemispheric climate dynamics and SST (**a**) Region 1 – 4 (**b**) Region 2 – 5 (**c**) Region 3 – 6. Precession shown in thick black line [2], thin black solid (dashed)-line represents Northern Hemisphere precipitation emulation (average proxy) record minus Southern Hemisphere precipitation emulation (average proxy) record and pink represents the average inter-hemispheric SST difference (low-latitude Northern Hemisphere – low-latitude Southern Hemisphere) calculated from proxy records (**d**). Due to the large

area covered by each region, including multiple ocean basins, we take an ad-hoc approach to comparing the inter-hemispheric SST difference with the inter-hemispheric hydroclimate (i.e. Region 1-4 is assigned the Pacific, Region 2-5 is assigned the Atlantic and Region 3-6 is assigned the Indian Ocean). (**d**) compilation of low-latitude SST records across MIS 5, interpolated onto a common 2 ka resolution. Low-latitude North Atlantic SST includes cores ODP 999A [3], MD03-2707 [4], MD02-2575 [5] and SO164-172 [6]; low-latitude South Atlantic SST includes cores GL-1090 [7], GeoB1028-5 [8], GeoB1016-3 [8], GeoB1105-4 [8] and M125-55-7/8 [9]; low-latitude North Pacific Ocean SST includes cores include ODP 1145 [10], IODP U1429 [11], TR163-22 [12], TR163-19 [13], MD02-2529 [14], ODP 1146 [15], ODP 806 [12], MD06-2067 [16] and ODP 871 [17]; low-latitude South Pacific SST includes cores MD98-2152 [18], MD06-3075 [19], MD05-2925 [20], SO18471[21] and MD01-2378 [22]; low-latitude North Indian Ocean includes SST record includes U1448 (this study), U1446 (this study), RC09-166 [23], SK157/4 [24], MD85674 [25], MD79257 [25] and TY93929/P [25]; low-latitude South Indian Ocean SST included cores SO139-74KL [26] and GeoB10038-4 [27].

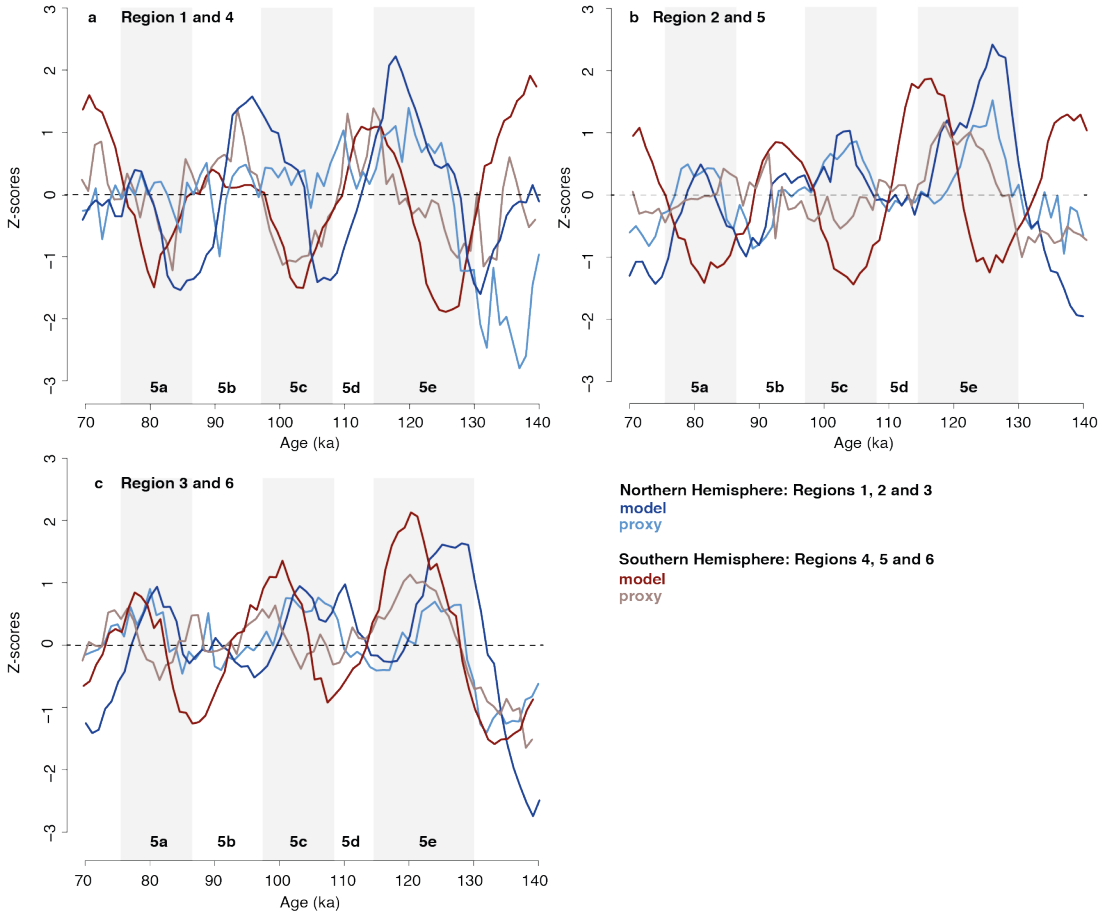

Supplementary Figure 5. Comparison of regions north and south of the equator to assess for hemispheric anti-phasing of hydroclimate (**a**) Region 1 – 4 (**b**) Region 2 – 5 (**c**) Region 3 – 6.

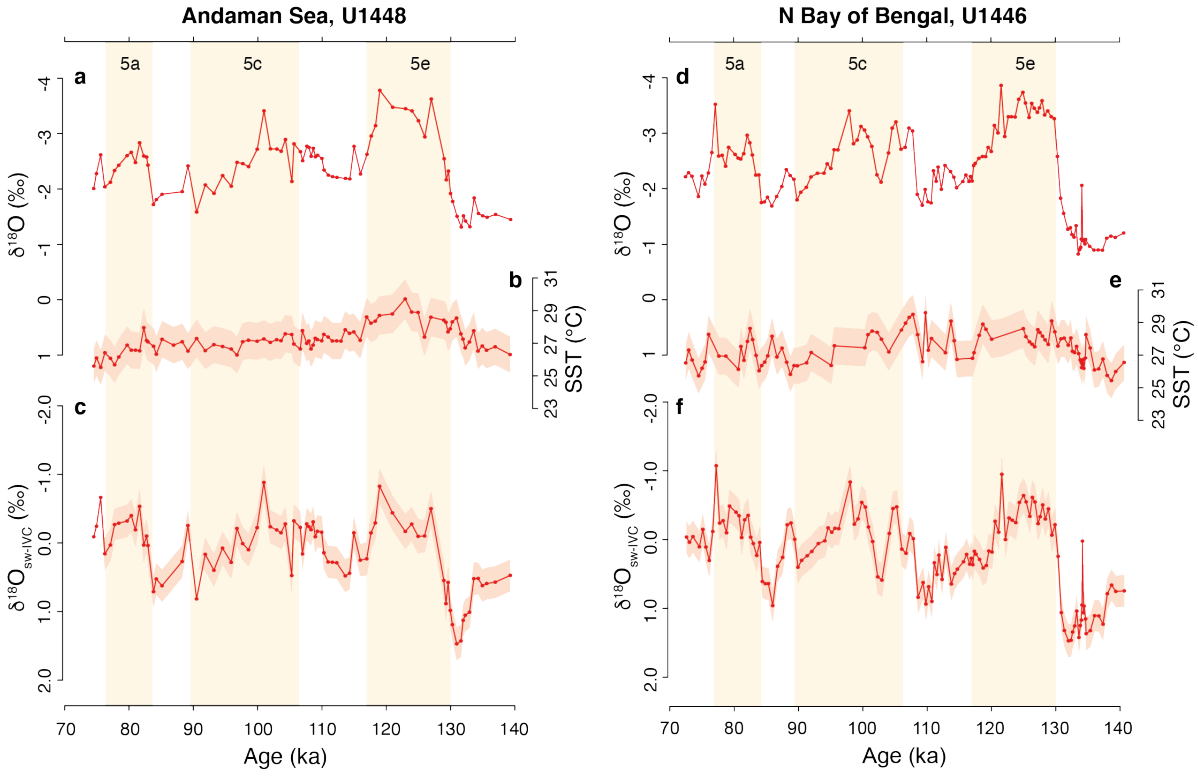

Supplementary Figure 6. *G ruber* ss proxy records generated in this study (**a**) U1448 *G. ruber ss* $\delta^{18}O$ (**b**) U1448 *G. ruber ss* Mg/Ca-derived SST (**c**) U1448 *G. ruber ss* $\delta^{18}O_{SW\text{-}IVC}$ (**d**) U1448 *G. ruber ss* $\delta^{18}O$ (**e**) U1448 *G. ruber ss* Mg/Ca-derived SST and (**f**) U1448 *G. ruber ss* $\delta^{18}O_{SW\text{-}IVC}$. Shaded areas represent 1σ.

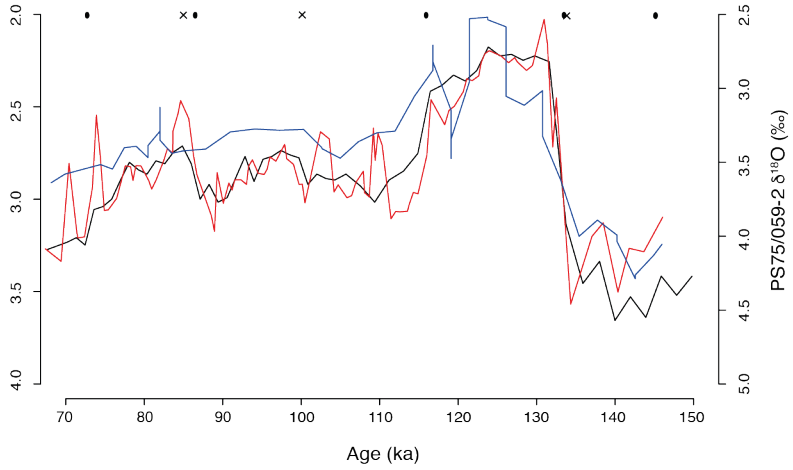

Supplementary Figure 7. Benthic $\delta^{18}O$ age-model for records generated in this study. U1446 (red) and U1448 (blue) benthic $\delta^{18}O$ age-model; core PS75/059-2 on AICC2012 chronology as the target [28,29]. Tie-points for U1446 as ellipses and crosses for U1448.

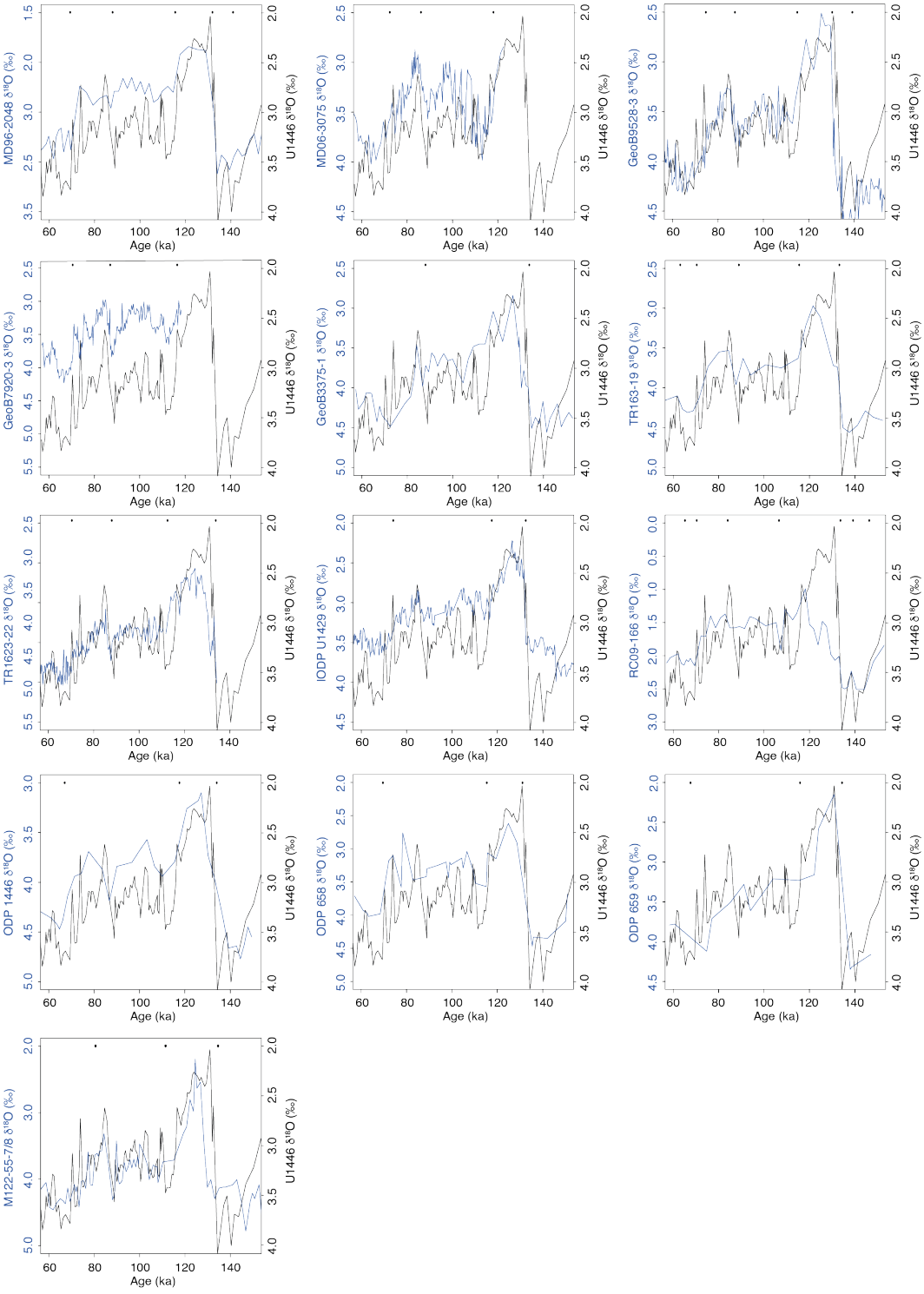

Supplementary Figure 8. New AICC2012 [30,31] benthic $\delta^{18}O$ age-models. U1446 as the target reference in black, black dots represent tie-points.

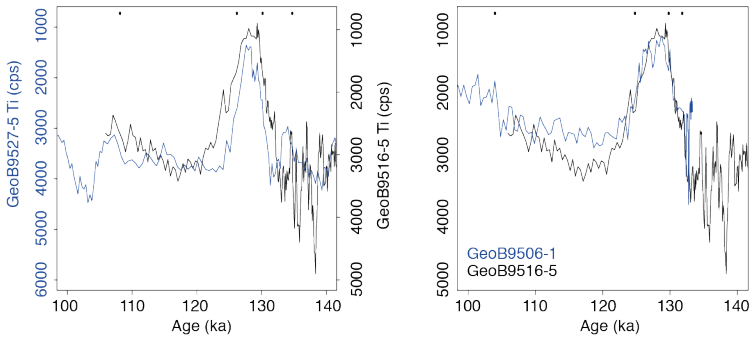

Supplementary Figure 9. New AICC2012 [30,31] age-models for cores GeoB9506-1 and GeoB0527-5 [32]. GeoB9516-5 as the target reference (black) [33], black dots represent tie-points.

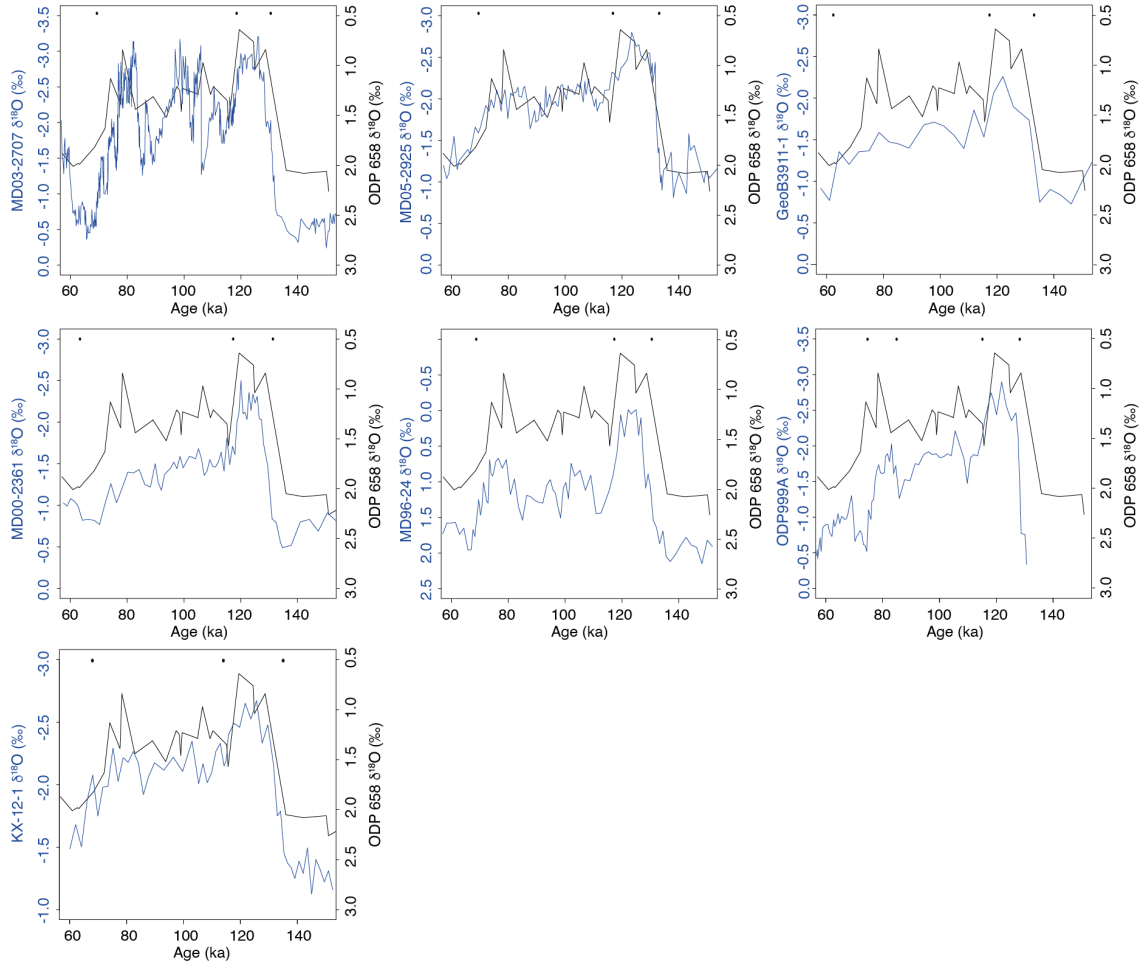

Supplementary Figure 10. New AICC2012 [30,31] planktic $\delta^{18}O$ age-models. ODP 658 [34] on AICC2012 chronology as the target reference in black, black dots represent tie-points.

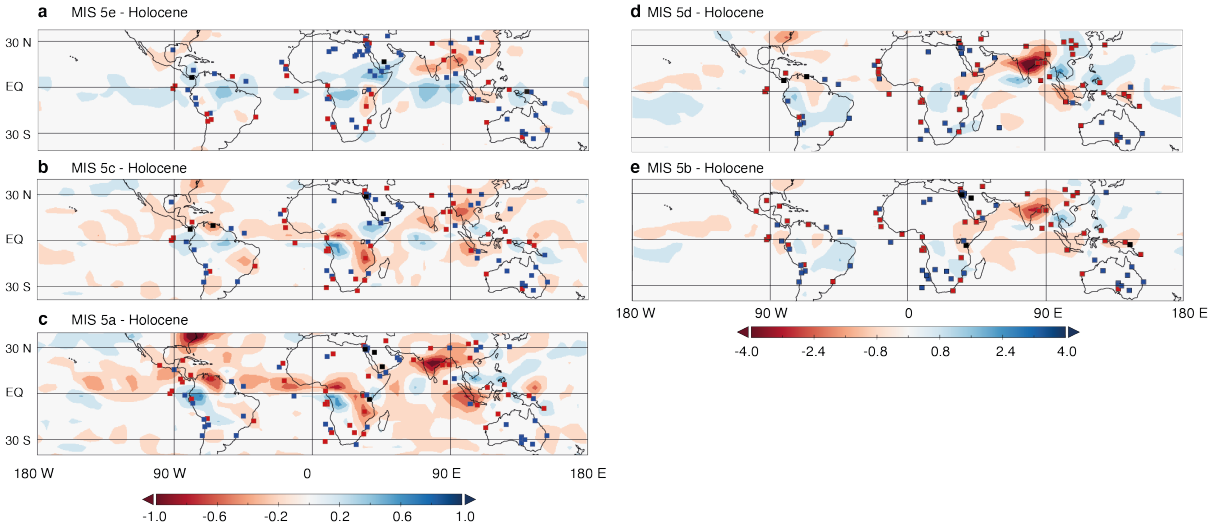

Supplementary Figure 11. Native PaleoPGEM resolution (64x32 grid cells) anomaly maps. Emulated anomaly maps of MIS 5 time-slices with respect to the Holocene (12-0 ka) with proxy data superimposed; blue square = "wetter" than Holocene average, red square = "drier" than Holocene average and black square = no change (Methods, Supplementary Data 1) (**a**) MIS 5e – Holocene (**b**) MIS 5c – Holocene (**c**) MIS 5a – Holocene (**d**) MIS 5d – Holocene (**e**) MIS 5b – Holocene. Maps were produced using Panoply (source: https://www.giss.nasa.gov/tools/panoply/).

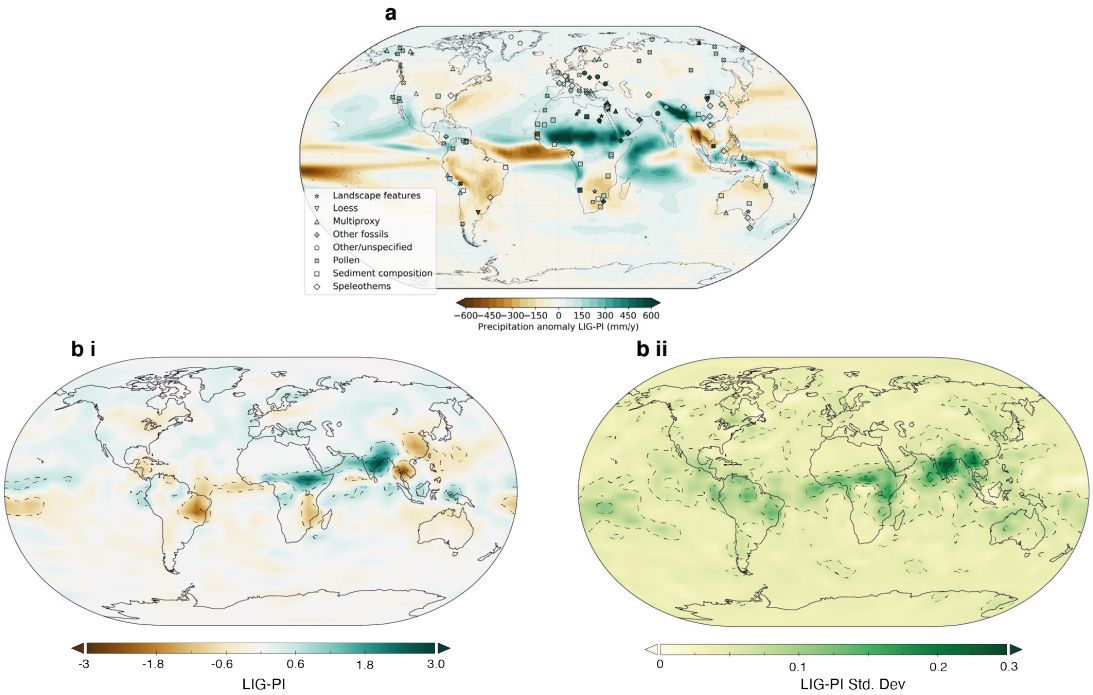

Supplementary Figure 12. Annual precipitation anomaly between the LIG (127 ka) – Preindustrial (PI) comparison (**a**) CMIP6-PMIP4 ensemble average [35] with proxy data compilation from [36] and (**b i**) PaleoPGEM mean and (**b ii**) PaleoPGEM standard deviation. Maps were produced using Panoply (source: https://www.giss.nasa.gov/tools/panoply/).

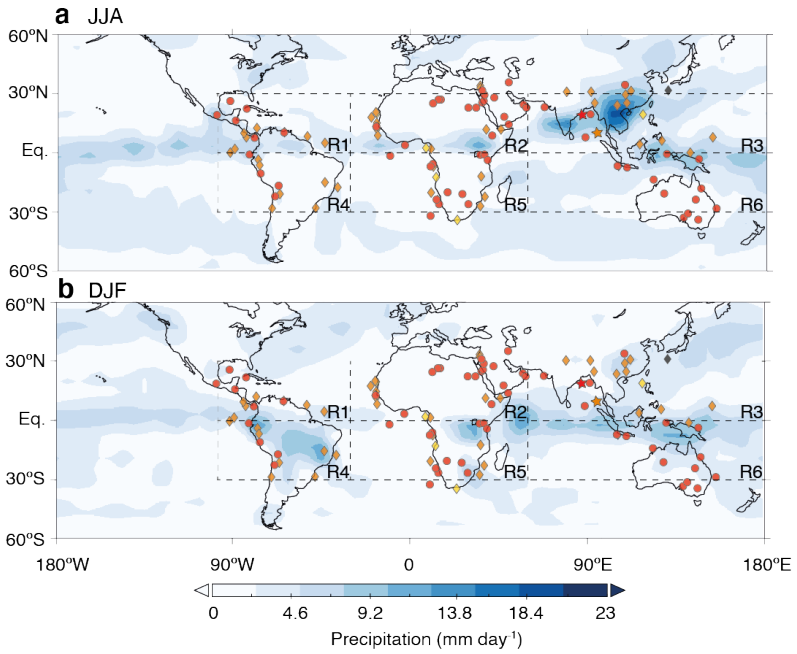

Supplementary Figure 13. Modern-day precipitation simulated by PLASIM-GENIE (**a**) June-July-August precipitation and (**b**) December-January-February precipitation**.** Map produced using Panoply (source: https://www.giss.nasa.gov/tools/panoply/).

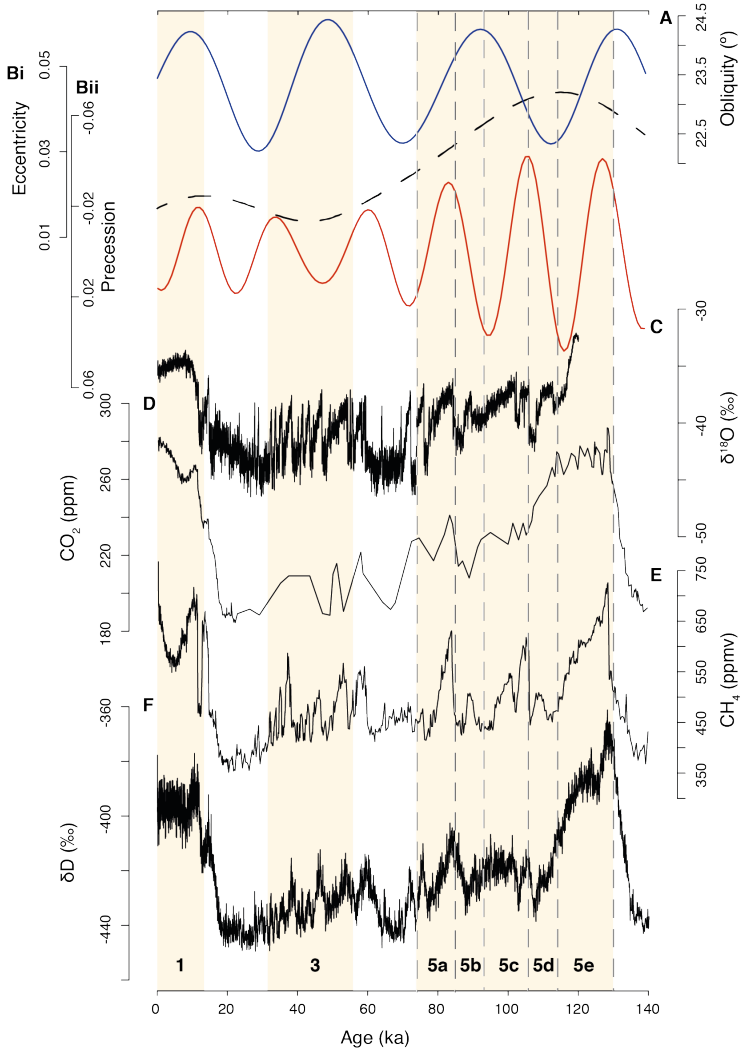

Supplementary Figure 14. Late Pleistocene climate records (**a**) Obliquity (blue) [2] (**b i**) Eccentricity (black dashed line) [2] (**b ii**) Precession (red) [2] (**c**) NGRIP $\delta^{18}O$ [37] (**d**) Antarctic composite CO_2 ice-core record [38] (**e**) EDC ice-core CH_4 [39] and (**f**) EDC ice-core δD [40]. All ice-core records are on AICC2012 chronology [30,31].

Supplementary References

1. Huang, E. *et al.* Dole effect as a measurement of the low-latitude hydrological cycle over the past 800 ka. *Sci. Adv.* **6,** eaba4823 (2020).
2. Laskar, J. *et al.* A long-term numerical solution for the insolation quantities of the Earth. *Astron. Astrophys.* **428,** 261–285 (2004).
3. Schmidt, M. W., Spero, H. J. & Lea, D. W. Links between salinity variation in the Caribbean and North Atlantic thermohaline circulation. *Nature* **428,** 160–163 (2004).
4. Weldeab, S., Lea, D. W., Schneider, R. R. & Andersen, N. 155,000 years of West African monsoon and ocean thermal evolution. *Science* **316,** 1303–1307 (2007).
5. Nürnberg, D., Ziegler, M., Karas, C., Tiedemann, R. & Schmidt, M. W. Interacting Loop Current variability and Mississippi River discharge over the past 400 kyr. *Earth Planet. Sci. Lett.* **272,** 278–289 (2008).
6. Bahr, A., Nürnberg, D., Schönfeld, J. & Garbe-Schönberg, D. Hydrological variability in Florida Straits during Marine Isotope Stage 5 cold events. *Paleoceanography* **26,** PA2214 (2011).
7. Santos, T. P. *et al.* Prolonged warming of the Brazil Current precedes deglaciations. *Earth Planet. Sci. Lett.* **463,** 1–12 (2017).
8. Schneider, R. R. *et al.* Sea-surface reconstruction of the east-equatorial South Atlantic: response to changes in trade/monsoon wind forcing and surface water avocation. in *The South Atlantic: Present and Past Circulation* (eds. Wefer, G., Berger, W. H., Siedler, G. & Webbs, D.) 527–551 (Springer, 1996).
9. Hou, A. *et al.* Forcing of western tropical South Atlantic sea surface temperature across three glacial-interglacial cycles. *Glob. Planet. Change* **188,** 103150 (2020).
10. Oppo, D. W. & Sun, Y. Amplitude and timing of sea-surface temperature change in the northern South China Sea: Dynamic link to the East Asian monsoon. *Geology* **33,** 785–788 (2005).
11. Clemens, S. C. *et al.* Precession-band variance missing from East Asian monsoon runoff. *Nat. Commun.* **9,** 3364 (2018).
12. Lea, D. W., Pak, D. K. & Spero, H. J. Climate Impact of Late Quaternary Equatorial Pacific Sea Surface Temperature Variations. *Science* **289,** 1719–1724 (2000).
13. Lea, D. W. *et al.* Paleoclimate history of Galápagos surface waters over the last 135,000 yr. *Quat. Sci. Rev.* **25,** 1152–1167 (2006).
14. Leduc, G. *et al.* Moisture transport across Central America as a positive feedback on abrupt climatic changes. *Nature* **445,** 908–911 (2007).
15. Thomas, E. K. *et al.* Temperature and leaf wax δ2H records demonstrate seasonal and regional controls on Asian monsoon proxies. *Geology* **42,** 1075–1078 (2014).
16. Bolliet, T. *et al.* Mindanao Dome variability over the last 160 kyr: Episodic glacial cooling of the West Pacific Warm Pool. *Paleoceanography* **26,** PA1208 (2011).
17. Dyez, K. A. & Ravelo, A. C. Late Pleistocene tropical Pacific temperature sensitivity to radiative greenhouse gas forcing. *Geology* **41,** 23–26 (2013).
18. Windler, G., Tierney, J. E., DiNezio, P. N., Gibson, K. & Thunell, R. Shelf exposure influence on Indo-Pacific Warm Pool climate for the last 450,000 years. *Earth Planet. Sci. Lett.* **516,** 66–76 (2019).
19. Fraser, N., Kuhnt, W., Holbourn, A., Bolliet, T. & Andersen, N. Precipitation variability within the West Pacific Warm Pool over the past 120 ka: evidence from offshore southern Mindano, Philippines. *Paleoceanography* **16,** 1094–1110 (2014).
20. Lo, L. *et al.* Nonlinear climatic sensitivity to greenhouse gases over past 4 glacial/interglacial cycles. *Sci. Rep.* **7,** 4626 (2017).
21. Lo Giudice Cappelli, E., Holbourn, A., Kuhnt, W. & Regenberg, M. Changes in Timor Strait hydrology and thermocline structure during the past 130 ka. *Palaeogeogr. Palaeoclimatol. Palaeoecol.* **462,** 112–124 (2016).
22. Xu, J., Holbourn, A., Kuhnt, W., Jian, Z. & Kawamura, H. Changes in the thermocline structure of the Indonesian outflow during Terminations I and II. *Earth Planet. Sci. Lett.* **273,** 152–162 (2008).
23. Tierney, J. E., deMenocal, P. B. & Zander, P. D. A climatic context for the out-of-Africa migration. *Geology* **45,** 1023–1026 (2017).
24. Saraswat, R., Nigam, R., Weldeab, S., Mackensen, A. & Naidu, P. D. A first look at past sea surface temperatures in the equatorial Indian Ocean from Mg/Ca in foraminifera. *Geophys. Res. Lett.* **32,** L24605 (2005).
25. Bard, E., Rostek, F. & Sonzogni, C. Interhemispheric synchrony of the last deglaciation inferred from alkenone palaeothermometry. *Nature* **385,** 707–710 (1997).
26. Lückge, A. *et al.* Monsoon versus ocean circulation controls on paleoenvironmental conditions off southern Sumatra during the past 300,000 years. *Paleoceanography* **24,** PA1208 (2009).
27. Mohtadi, M. *et al.* Late Pleistocene surface and thermocline conditions of the eastern tropical Indian

Ocean. *Quat. Sci. Rev.* **29,** 887–896 (2010).
28. Ullermann, J. *et al.* Pacific-Atlantic Circumpolar Deep Water coupling during the last 500 ka. *Paleoceanography* **31,** 639–650 (2016).
29. Lamy, F. *et al.* Increased dust deposition in the Pacific Southern Ocean during glacial periods. *Science* **343,** 403–407 (2014).
30. Veres, D. *et al.* The Antarctic ice core chronology (AICC2012): an optimized multi-parameter and multi-site dating approach for the last 120 thousand years. *Clim. Past* **9,** 1733–1748 (2013).
31. Bazin, L. *et al.* An optimized multi-proxy, multi-site Antarctic ice and gas orbital chronology (AICC2012): 120-800 ka. *Clim. Past* **9,** 1715–1731 (2013).
32. Itambi, A. C., von Dobeneck, T., Mulitza, S., Bickert, T. & Heslop, D. Millennial-scale northwest African droughts related to Heinrich events and Dansgaard-Oeschger cycles: Evidence in marine sediments from offshore Senegal. *Paleoceanography* **24,** PA1205 (2009).
33. Govin, A., Varma, V. & Prange, M. Astronomically forced variations in western African rainfall (21°N-20°S) during the Last Interglacial period. *Geophys. Res. Lett.* **41,** 2117–2125 (2014).
34. Sarnthein, M. & Tiedemann, R. Toward a High-Resolution Stable Isotope Stratigraphy of the Last 3.4 Million Years: Sites 658 and 659 off Northwest Africa. in *Proceedings of the Ocean Drilling Program, 108 Scientific Results* (Ocean Drilling Program, 1989). doi:10.2973/odp.proc.sr.108.159.1989
35. Otto-bliesner, B. L. *et al.* Large-scale features of Last Interglacial climate : results from evaluating the lig127k simulations for the Coupled Model Intercomparison Project (CMIP6)– Paleoclimate Modeling Intercomparison Project (PMIP4). *Clim. Past* **17,** 63–94 (2021).
36. Scussolini, P. *et al.* Agreement between reconstructed and modeled boreal precipitation of the Last Interglacial. *Sci. Adv.* **5,** eaax7047 (2019).
37. Andersen, K. K. *et al.* High-resolution record of Northern Hemisphere climate extending into the last interglacial period. *Nature* **431,** 147–151 (2004).
38. Lüthi, D. *et al.* High-resolution carbon dioxide concentration record 650,000–800,000 years before present. *Nature* **453,** 379–382 (2008).
39. Loulergue, L. *et al.* Orbital and millennial-scale features of atmospheric CH_4 over the past 800,000 years. *Nature* **453,** 383–386 (2008).
40. Jouzel, J. *et al.* Orbital and millennial Antarctic climate variability over the past 800,000 years. *Science* **317,** 793–796 (2007).